

1 Visual and auditory cortices represent acoustic speech-related 2 information during silent lip reading

3 Felix Bröhl^{1*}, Anne Keitel², Christoph Kayser¹

4 ¹*Department for Cognitive Neuroscience, Faculty of Biology, Bielefeld University, Universitätsstr. 25, 33615, Bielefeld, Germany*

5 ²*Psychology, University of Dundee, Scrymgeour Building, Dundee DD1 4HN, UK*

6 * **Corresponding author:** Felix Bröhl (felix.broehl@uni-bielefeld.de)

7 Highlights

- 8 ● Visual and auditory cortex represent unheard acoustic information during lip reading
- 9 ● Auditory cortex emphasizes the acoustic envelope
- 10 ● Visual cortex emphasizes a pitch signature
- 11 ● Tracking of unheard features in auditory cortex is associated with behavior

12 Abstract

13 Speech is an intrinsically multisensory signal and seeing the speaker's lips forms a cornerstone of
14 communication in acoustically impoverished environments. Still, it remains unclear how the brain exploits
15 visual speech for comprehension and previous work debated whether lip signals are mainly processed along
16 the auditory pathways or whether the visual system directly implements speech-related processes. To probe
17 this question, we systematically characterized dynamic representations of multiple acoustic and visual
18 speech-derived features in source localized MEG recordings that were obtained while participants listened
19 to speech or viewed silent speech. Using a mutual-information framework we provide a comprehensive
20 assessment of how well temporal and occipital cortices reflect the physically presented signals and speech-
21 related features that were physically absent but may still be critical for comprehension. Our results
22 demonstrate that both cortices are capable of a functionally specific form of multisensory restoration: during
23 lip reading both reflect unheard acoustic features, with occipital regions emphasizing spectral information
24 and temporal regions emphasizing the speech envelope. Importantly, the degree of envelope restoration was
25 predictive of lip reading performance. These findings suggest that when seeing the speaker's lips the brain
26 engages both visual and auditory pathways to support comprehension by exploiting multisensory
27 correspondences between lip movements and spectro-temporal acoustic cues.

28 **Keywords**

29 Speech entrainment, lip-reading, audio-visual, speech tracking, language, MEG

30

31 **1. Introduction**

32 Speech is an intrinsically multisensory stimulus that is often conveyed via both acoustic and visual signals.
33 Visual speech contains information that becomes particularly important in circumstances when the acoustic
34 signal is impoverished, such as by background noises or distractors (Ross et al., 2007; Sumbly and Pollack,
35 1954). In these cases listeners typically look at the speaker's face to achieve a genuine multisensory benefit
36 for comprehension, which in the brain is mediated by an enhanced cortical encoding of acoustic and
37 phonemic speech features (Giordano et al., 2017; Mégevand et al., 2020; O'Sullivan et al., 2017; Zion
38 Golumbic et al., 2013). However, in situations where only visual speech cues are available, i.e. during silent
39 lip reading, visual signals allow comprehension also when the respective acoustic information is absent (Besle
40 et al., 2008; Calvert et al., 1997; Calvert and Campbell, 2003; Grant and Seitz, 2000).

41 How exactly the brain represents the information derived from visual speech and how it exploits this for
42 comprehension remains debated. One possibility is that visual speech is represented in regions of the
43 auditory pathways, possibly exploiting speech-specific processes of the auditory system. Neuroimaging
44 studies support this view by demonstrating the activation of the auditory cortex when participants view the
45 articulation of words or pseudo-words, but not when viewing non-speech gestures (Bernstein et al., 2002;
46 Besle et al., 2008; Calvert et al., 1997; Calvert and Campbell, 2003; Pekkola et al., 2005; Sams et al., 1991).
47 Along this line, a recent study has suggested that the auditory cortex can reflect the unheard acoustic
48 envelope of a spoken narrative (Bourguignon et al., 2020), presumably because auditory regions restore this
49 temporal speech-related signature from the seen trajectory of the lip movements. Given that the
50 representation of speech signals in temporally-aligned neural activity is essential for comprehension
51 (Brodbeck and Simon, 2020; Giraud and Poeppel, 2012; Obleser and Kayser, 2019), this can be seen as indirect
52 evidence that the auditory system supports lip reading by restoring key signatures of the underlying acoustic
53 information based on the visual input.

54 Another view is that the visual system directly contributes to establishing speech representations separately
55 from those established along the auditory pathway (Bernstein et al., 2011; O'Sullivan et al., 2017; Ozker et
56 al., 2018). Visual speech contains temporal information that can be predictive of subsequent acoustic signals
57 and allows mapping visual cues onto phonological representations (Campbell, 2008; Lazard and Giraud,
58 2017). Importantly, the visual cortex tracks dynamic lip signals (Park et al., 2016) and, as suggested recently,
59 may also restore the unheard acoustic envelope of visually presented speech (Hauswald et al., 2018; Suess
60 et al., 2022). Importantly, the evidence that visual speech induces information about the unheard speech
61 acoustics along both auditory and the visual pathways may not be mutually exclusive, as both may contribute
62 to a supramodal frame of reference for speech (Arnal et al., 2009; Rauschecker, 2012).

63 Many questions concerning a potential duality of acoustic speech-related representations during silent lip
64 reading remain open (Bernstein and Liebenthal, 2014). First, each putative representation (in auditory and in
65 visual cortex) was reported in a separate study and may have emerged mainly due to the specific stimuli or

66 the specific analysis approach that was being applied (Bourguignon et al., 2020; Hauswald et al., 2018).
67 Hence, it remains unclear whether both auditory and visual regions reflect acoustic speech features in
68 parallel. Second, previous studies mainly capitalized on one-dimensional characterizations of the relevant
69 sensory signals, such as the broadband speech envelope or the lip aperture. However, the cerebral encoding
70 of speech is intrinsically multidimensional, and reflects temporal acoustic features such as the overall
71 envelope or its derivative and spectral features such as pitch (Metzger et al., 2020; O'Sullivan et al., 2017;
72 Oganian and Chang, 2019; Teoh et al., 2019). This raises the question of whether the previously observed
73 restoration of acoustic speech-related information is tied to specific features, i.e. whether auditory regions
74 preferentially encode the speech envelope or spectral features during lip reading. Third, it remains unclear
75 whether a genuine acoustic feature is indeed represented independently of the physically observed lip
76 movements and vice-versa. Alternatively, it may be previously reported restoration effects are largely
77 explained by encoding of amodal information shared between both visual and acoustic modalities, which
78 could be relayed to early sensory regions mainly by top-down processes. And finally, the behavioral relevance
79 of the cerebral encoding of auditory speech features during lip reading remains unclear, as previous work
80 mostly focused on neural signals but did not obtain direct measures of speech perception in natural language
81 at the same time.

82 We systematically probed dynamic representations of acoustic and visual speech-related features in
83 temporal and occipital brain regions during listening and viewing speech in the same participants using a
84 mutual information approach (Daube et al., 2019; Keitel et al., 2018). This allowed us to provide a
85 comprehensive assessment of how well temporal and occipital regions reflect either acoustic speech features
86 or information about the lip trajectory, independently of each other, and both during hearing purely acoustic
87 speech or while only seeing the speaker (lip reading). We probed the four main questions outlined above and
88 found that both regions reflect unheard acoustic speech-related features independently of the physically
89 observed lip movements. This 'restoration' of acoustic information in the temporal, but not the occipital,
90 cortex was predictive of comprehension performance across participants.

91 **2. Materials and Methods**

92 The data analyzed in this study has been collected and analyzed in previous studies (Keitel et al., 2020, 2018).
93 The analyses conducted here pose new questions and provide novel results beyond the previous work.

94 **2.1 Participants and data acquisition**

95 Data was collected from 20 native English speaking participants (9 female, age 23.6 ± 5.8 years mean \pm SD).
96 Due to prominent environmental artefacts in the MEG recordings, data from two participants were excluded
97 from further analysis. Thus, the analyzed data is from 18 participants (7 female). All participants were
98 screened for hearing impairment prior to data collection (Koike et al., 1994), had normal or corrected-to-

99 normal vision and were all right-handed (Oldfield, 1971). All participants provided written informed consent
100 and received monetary compensation of 10£/h. The experiment was approved by the College of Science and
101 Engineering, University of Glasgow (approval number 300140078) and conducted in compliance with the
102 Declaration of Helsinki.

103 MEG data was collected using a 248-magnetometer whole-head MEG system (MAGNES 3600 WH, 4-D
104 Neuroimaging) with a sample rate of 1 kHz. Head positions were measured at the beginning and end of each
105 run, using five coils placed on the participants' heads. Coil positions were co-digitized with the participant's
106 head-shape (FASTRAK®, Polhemus Inc., VT, USA). Participants were seated in an upright position in front of a
107 screen. Visual stimuli were displayed with a DLP projector at 25 frames per second, a resolution of 1280 ×
108 720 pixels, and covered a visual field of 25 × 19 degrees. Acoustic stimuli were transmitted binaurally through
109 plastic earpieces and 370-cm long plastic tubes connected to a sound pressure transducer and were
110 presented in stereo at a sampling rate of 22,050 Hz.

111 **2.2 Stimulus material**

112 The stimulus material comprised two structurally equivalent sets of 90 unique matrix-style English sentences.
113 Each sentence was constructed with the same sequence of linguistic elements, the order of which can be
114 described with the following pattern [filler phrase, time phrase, name, verb, numeral, adjective, noun]. One
115 such sentence for example was 'I forgot to mention (filler phrase), last Thursday morning (time phrase) Marry
116 (name) obtained (verb) four (numeral) beautiful (adjective) journals (noun)'. For each element, a list of 18
117 different options was created and sentences were constructed so that each single element was repeated ten
118 times. Sentence elements were randomly combined within each set of 90 sentences. To measure
119 comprehension performance for each sentence, a target word was defined in each sentence: either the
120 adjective (first set of sentences) or the numeral (second set). Sentences lasted on average 5.4 ± 0.4 s (mean
121 \pm SD, ranging from 4.6 s to 6.5 s) and lasted a total of approximately 22 minutes. The speech material was
122 spoken by a male British actor, who was tasked to speak clearly and naturally and to move as little as possible
123 while speaking to assure that the lips center stayed at the same place in each video frame. Audiovisual
124 recordings were gathered with a high-performance camcorder (Sony PMW-EX1) and an external microphone
125 in a sound attenuating booth.

126 Participants were presented with audio-only (A), audiovisual (AV) or visual-only (V) speech material in three
127 conditions (Keitel et al., 2018). However, for the present analysis we only focus on the A and V conditions, as
128 in these one can best dissociate visual- and auditory-related speech representations given that only one
129 physical stimulus was present. Furthermore, during the AV condition comprehension performance was near-
130 ceiling (Keitel et al., 2020), making it difficult to link cerebral and behavioral data. To match the behavioral
131 performance in the A and V condition, the acoustic speech was embedded in environmental noise. The noise
132 for each trial was generated by randomly selecting 50 individual sounds from a set of sounds recorded from

133 natural, everyday sources or scenes (e.g. car horns, talking people, traffic). For each participant the individual
134 noise level was adjusted, as described previously (Keitel et al., 2020).

135 **2.3 Experimental Design**

136 Each participant was presented with each of the 180 sentences in three conditions (A, V and AV). The order
137 of the conditions was fixed for all participants as A, AV and then V. Each condition was divided into 4 blocks
138 of 45 sentences each, with two blocks being 'adjective' and two 'number' blocks. For each participant, the
139 order of sentences within each block was randomized. The first sentence of each block was a 'dummy' trial
140 that was subsequently excluded from analysis. During each trial, participants either fixated a dot (in A
141 condition) or a small cross overlaid onto the mouth of the speaker's face (in V condition). In the A condition,
142 each sentence was presented as the respective audio recording, i.e. the spoken sentence, together with the
143 background noise. In the V condition, only the video of the speaker's face was presented and no sound was
144 present. After each trial, four response option words (either adjectives or written numbers) were presented
145 on the screen and participants had to indicate using a button press which word they had perceived. Inter-
146 trial intervals were set to last about two seconds.

147 **2.4 Preprocessing of stimulus material**

148 From the stimulus material we extracted the following auditory and visual features. In the auditory domain,
149 we derived the broadband envelope, the slope of the broadband envelope and the pitch contour. To derive
150 the broadband envelope we filtered the acoustic waveform into twelve logarithmically spaced bands
151 between 0.1 and 10 kHz (zero-phase 3rd order Butterworth filter with boundaries: 0.1, 0.22, 0.4, 0.68, 1.1,
152 1.7, 2.7, 4.2, 6.5, 10 kHz) and subsequently took the absolute value of the Hilbert transform for each band
153 (Bröhl and Kayser, 2020). The broadband amplitude envelope was then derived by taking the average across
154 all twelve band-limited envelopes and was subsequently down-sampled to 50 Hz. We computed the slope of
155 this broadband envelope by taking its first derivative (Oganian and Chang, 2019). To characterize the pitch
156 contour we extracted the fundamental frequency over time using the Praat software ('to Pitch' method with
157 predefined parameters) (Boersma and van Heuven, 2001). This was done using the original acoustic
158 waveform at a sampling rate of 22,050 Hz. The resulting pitch contour was again down sampled to 50 Hz. All
159 three acoustic features together are labelled *AudFeat* in the following.

160 From the video recordings we derived the horizontal and vertical opening of the lips, the area covered by the
161 lip opening, and its derivative. The lips were extracted based on the color of the lips in the video material
162 using a custom-made algorithm. From these we determined the contour of the lip opening based on
163 luminance values and deriving connected components from these (Giordano et al., 2017). The results were
164 visually inspected to ensure accurate tracking of the lips. From this segmentation of the lip opening we
165 derived the total opening (in pixels) and estimates of the respective diameters along the horizontal and
166 vertical axes: these were defined between the outermost points along the respective horizontal (vertical)

167 axis. These signals were initially sampled at the video rate of 30 fps. As for the auditory features, we
168 computed the slope of the lip area. The time series of these visual features were then linearly interpolated
169 to a sample rate of 50 Hz. Because the horizontal and vertical mouth openings are partially correlated with
170 each other and with the total mouth opening, we selected the total area and the horizontal width as signals
171 of interest, as the latter is specifically informative about the acoustic formant structure (Plass et al., 2020).
172 We grouped the total lip area, its temporal derivative and the lip-width as signatures of lip features (*LipFeat*),
173 which are of the same dimensionality as the acoustic features (*AudFeat*) described above.

174 For each of these features we derived its power spectrum and cross-coherence with the other features using
175 MATLAB's 'pwelch' and 'mscoher' functions using a window length of 3 s with 50% overlap and otherwise
176 predefined parameters. The resulting spectra were log transformed and averaged across sentences. To
177 visualize the cross-coherences we first obtained key frequency ranges of interest from our main results (c.f.
178 Fig. 3) and averaged the coherences within two ranges of interest (0.5 - 1 Hz and 1 - 3 Hz). This was done to
179 illustrate the stimuli's spectral properties in the relevant frequency ranges.

180 **2.5 MEG preprocessing**

181 Preprocessing of MEG data was carried out using custom MATLAB scripts and the FieldTrip toolbox
182 (Oostenveld et al., 2011). Each experimental block was processed separately. Individual trials were extracted
183 from continuous data starting 2 s before sound onset and until 10 s after sound onset. The MEG data were
184 denoised using a reference signal. Known faulty channels (N=7) were removed. Trials with SQUID jumps (3.5%
185 of trials) were detected and removed using FieldTrip procedures with a cut-off z-value of 30. Data were band-
186 pass filtered between 0.2 and 150 Hz using a zero-phase 4th order Butterworth filter and subsequently down
187 sampled to 300 Hz before further artefact rejection. Data were visually inspected to find noisy channels (4.37
188 ± 3.38 on average across blocks and participants) and trials (0.66 ± 1.03 on average across blocks and
189 participants). Noise cleaning was performed using independent component analysis with 30 principal
190 components (2.5 components removed on average). Data were further down sampled to 50 Hz and bandpass
191 filtered between 0.8 and 30 Hz using a zero-phase 3rd order Butterworth filter for subsequent analysis.

192 **2.6 MEG source reconstruction**

193 Source reconstruction was performed using Fieldtrip, SPM8, and the Freesurfer toolbox based on T1-
194 weighted structural magnetic resonance images (MRIs) for each participant. These were co-registered to the
195 MEG coordinate system using a semi-automatic procedure (Gross et al., 2013; Keitel et al., 2017). MRIs were
196 then segmented and linearly normalized to a template brain (MNI space). We projected sensor-level time
197 series into source space using a frequency-specific linear constraint minimum variance (LCMV) beamformer
198 (Van Veen et al., 1997) with a regularization parameter of 7% and optimal dipole orientation (singular value
199 decomposition method). The grid points had a spacing of 6 mm, thus resulting in 12,337 points. For whole-
200 brain analyses, a subset of grid points corresponding to cortical gray matter regions only was selected (using

201 the AAL atlas, Tzourio-Mazoyer et al., 2002), yielding 6,490 points in total. Within these we defined auditory
202 and visual regions of interest (ROI) based on the brainnetome atlas (Yu et al., 2011). The individual ROIs were
203 chosen based on previous studies that demonstrate the encoding of acoustic and visual speech features in
204 occipital and superior temporal regions (Di Liberto et al., 2018; Giordano et al., 2017; Keitel et al., 2020; Teng
205 et al., 2018). As auditory ROI we included Brodmann area 41/42, caudal area 22 (A22c), rostral area 22 (A22r)
206 and TE1.0 and TE1.2. As visual ROI we defined the middle occipital gyrus (mOccG), occipital polar gyrus (OPC),
207 inferior occipital gyrus (iOccG) and the medial superior occipital gyrus (msOccG).

208 **2.7 MEG analysis**

209 Source reconstructed MEG data were analyzed using a mutual information (MI) framework (Ince et al., 2017).
210 The analysis relies on the notion that a significant temporal relation between cerebral signal and sensory
211 features is indicating the cerebral encoding (or tracking) of the respective features by temporally entrained
212 brain activity (Bröhl and Kayser, 2020; Keitel et al., 2018; Park et al., 2016). In the following we use the term
213 ‘tracking’ when referring to such putative cerebral representations characterized using MI (Obleser and
214 Kayser, 2019). To quantify the tracking of a given stimulus feature, or of a feature group, we concatenated
215 the trial-wise MEG data and features along the time dimension and filtered these (using 3rd order
216 Butterworth IIR filters) into typical frequency bands used to study dynamic speech encoding: 0.5 - 1 Hz, 1 - 3
217 Hz, 2 - 4 Hz, 3 - 6 Hz and 4 - 8 Hz (and 0.5 - 8 Hz). These were chosen based on previous work (Bröhl and
218 Kayser, 2020; Etard and Reichenbach, 2019; van Bree et al., 2020; Zuk et al., 2021). The first 500 ms of each
219 sentence were discarded to remove the influence of the transient sound-onset response. To compute the MI
220 between filtered MEG and stimulus features, we relied on a complex-valued representation of each signal,
221 which allowed us to include both the amplitude and phase information in the analysis: we first derived the
222 analytic signal of both the MEG and stimulus feature(s) using the Hilbert transform and then calculated the
223 MI using the Gaussian copula approach including the real and imaginary part of the Hilbert signals (Daube et
224 al., 2019; Ince et al., 2017).

225 In a first step, we used this framework to visualize the tracking of AudFeat and LipFeat within the entire
226 source space. This was mainly done to assert that the predefined ROIs used for the subsequent analysis
227 indeed covered the relevant tracking of these features (Fig. 2). This analysis relied on a frequency range from
228 0.5 to 8 Hz and a range of stimulus-to-brain lags from 60 to 140 ms after stimulus onset. For the main analysis,
229 we quantified the tracking of auditory or visual features and their dependencies specifically in each ROI (Fig.
230 3,4,5). To facilitate these analyses, we first determined the optimal lags for each feature, ROI and frequency
231 band, given that the encoding latencies may differ between features and regions (Giordano et al., 2017). For
232 this we determined at the group-level and for each feature group (i.e. AudFeat and LipFeat) and for each ROI
233 and frequency band the respective lag yielding the largest group-level MI value (across participants and both
234 A only and V only trials): for this we probed a range of lags between 0 and 500 ms in 20 ms steps. For the

235 subsequent analyses, we used these optimal lags and averaged MI values obtained in a time window of -60
236 to 60 ms around these lags (computed in 20 ms steps).

237 Our hypotheses concerned both the MI between each feature group and the MEG and the statistical
238 dependence of the tracking of each group on the tracking of the respective other group. To address this
239 dependency, we determined whether the tracking of each feature group (in a given ROI and frequency band)
240 is statistically redundant with (or possibly complementary to) the other group. For this we calculated the
241 conditional MI between MEG and one feature group, partialling out the respective other group (Fig. 3, CMI
242 values) (Giordano et al., 2017; Ince et al., 2017). Similarly, we also determined the conditional MI between
243 the MEG and each individual feature, obtained by partialling out all other visual and auditory features (Fig.
244 4). To be able to compare the MI and CMI estimates directly, we ensured that both estimates had comparable
245 statistical biases. To achieve this, we effectively derived the MI as a conditional estimate, in which we
246 partialled out a statistically-unrelated variable. That is, we defined

$$247 \quad MI(\text{feature} ; \text{MEG}) \cong MI(\text{feature} ; \text{MEG} | \text{time_shifted_feature})$$

248 Here, *time_shifted_feature* is a representation of the respective feature(s) with a random time lag and hence
249 no expected causal relation to the MEG. Each MI estimate was obtained by averaging this estimate over 2,000
250 repeats of a randomly generated time-shifted feature vector. To render the (conditional) MI estimates
251 meaningful relative to the expectation of zero MI between MEG and stimulus features, we furthermore
252 subtracted an estimate of the null-baseline of no systematic relation between signals. This was obtained by
253 computing (conditional) MI values after randomly time-shifting the stimulus feature(s) and averaging the
254 resulting surrogate MI estimates over 100 randomizations.

255 **2.8 Relating MI to comprehension performance**

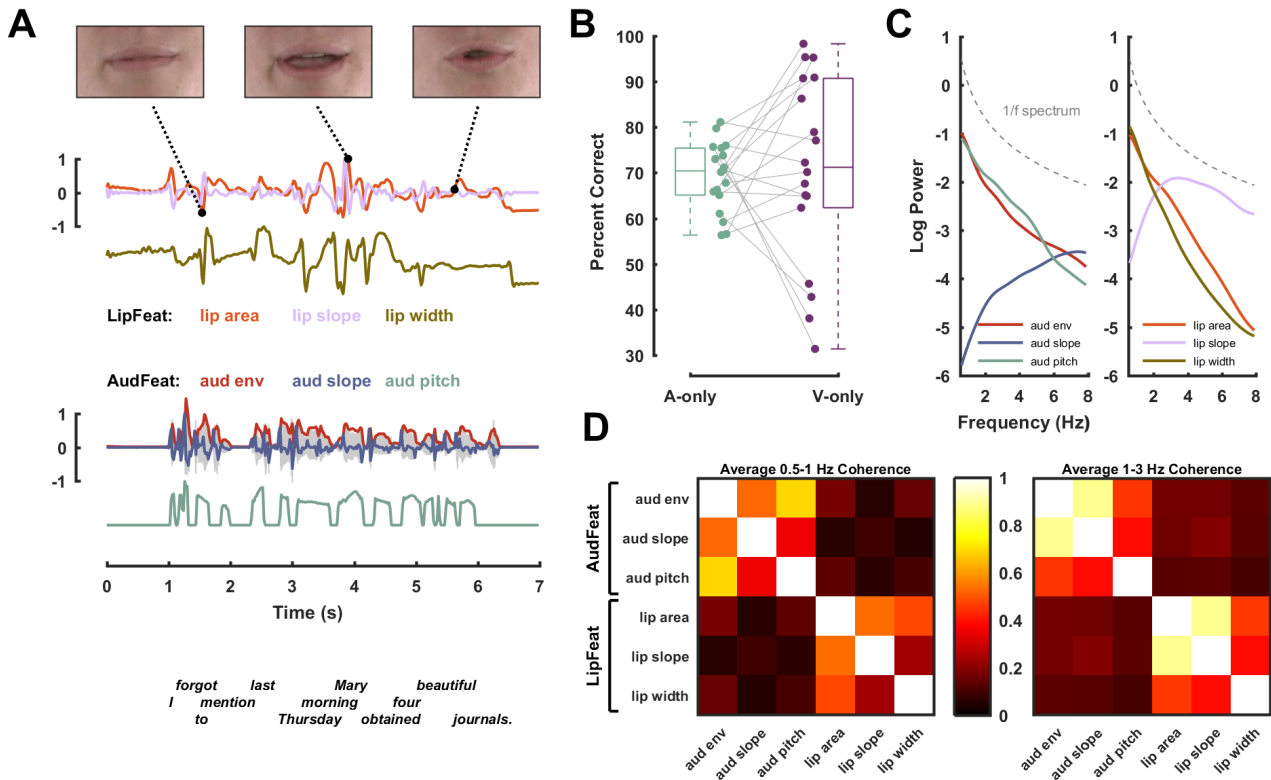
256 The behavioral performance for each participant and condition was obtained as the percent correctly (PC)
257 reported target words (obtained in a 4-choice task). To relate the tracking of specific features to
258 comprehension performance, we accounted for potential spurious correlations between these due to the
259 respective signal-to-noise ratio in each participants' dataset. This was implemented using multiple
260 regression, in which we predicted the PC in the visual trials based on i) the individual MI for *aud env* in the
261 temporal ROI and the MI for *aud pitch* in the and occipital ROI as the primary variables of interest, and ii) the
262 tracking of LipFeat (MI) in the occipital ROI in visual trials and iii) the tracking of AudFeat in the temporal ROI
263 in auditory trials. The last two serve as potentially confounding variables, as they provide a proxy to the
264 overall SNR of the speech and lip tracking in the respective dataset. By focusing on *aud env* / *aud pitch* in the
265 temporal / occipital ROIs respectively, we predicted task performance based on the individual features that
266 were most associated with the tracking of AudFeat (c.f. Fig. 4B,C). To establish these regression models, we
267 z-scored the MI values of interest (variables i - iii) and the PC across participants. For the confounding
268 variables, we applied the z-scoring for each frequency band and subsequently averaged the z-scored values
269 across bands. For each frequency band, we created a single model containing all target and confounding

270 variables. From the respective models we obtained the significance of each predictor of interest.
271 Furthermore, we compared the predictive power of this full model with that of a reduced model not featuring
272 the predictors of interest (variable *i*). From the likelihoods of each model we derived the relative Bayes factor
273 (BF) between these based on the respective BIC values obtained from each model. For visualization we used
274 partial residual plots using the procedure described by Velleman and Welsch (Velleman and Welsch, 1981).
275 This procedure was applied to each individual feature of interest (i.e. *aud env* and *aud pitch*).

276 **2.9 Statistical analysis**

277 Statistical testing was based on a non-parametric randomization approach incorporating corrections for
278 multiple comparisons (Nichols and Holmes, 2003). To test whether the group-level median MI (or CMI) values
279 were significantly higher than expected based on the null hypothesis of no systematic temporal relation
280 between sensory features and MEG, we proceeded in a similar fashion as in previous work (Bröhl and Kayser,
281 2020; Giordano et al., 2017): we obtained a distribution of 2,000 MI values between randomly time-shifted
282 MEG and the stimulus vectors, while keeping the temporal relation of individual features to each other
283 constant. This distribution was obtained for each participant, frequency band, feature (AudFeat and LipFeat),
284 ROI (temporal, occipital) and condition (A-only, V-only) separately. To correct for multiple comparisons, we
285 generated a maximum distribution across all dimensions except frequency bands, given that the MI values
286 decreased considerably across bands (c.f. Fig. 3). We then tested the group-level median against the 99th
287 percentile of this maximum distribution as a significance threshold, which effectively implements a one-sided
288 randomization test at $p < 0.01$ corrected for all dimensions except frequency bands. To test for differences
289 between MI and CMI values for a given condition, band and ROI, we also used a permutation approach
290 combined with a Wilcoxon signed-rank test: first, we established the respective true Wilcoxon z-statistic
291 between MI and CMI values; then we created a distribution of surrogate z-statistics under the null hypothesis
292 of no systematic group-level effect, obtained by randomly permuting the labels of MI and CMI values 5,000
293 times. From this we obtained the maximum across features, bands, ROIs and conditions to correct for
294 multiple comparisons and used the 99th percentile of this randomization distribution to determine the
295 significance of individual tests.

296 The CMI values for individual features in Figure 4 were compared using a one-way repeated measure Kruskal-
297 Wallis rank test, followed by a post-hoc Tukey Kramer multiple comparison. We used the same procedure to
298 test for differences between CMI values in the sub-areas composing each ROI (Table 1). To test CMI values
299 between hemispheres, we used a Wilcoxon signed rank test (Table 2). The resulting p-values were corrected
300 for false discovery rate using the Benjamini-Hochberg procedure within each set of comparisons (Benjamini
301 and Hochberg, 1995). In all tests an alpha level of $\alpha < 0.01$ was deemed significant. For all statistical tests we
302 provide exact p-values, except for randomization tests where the approximate p-values were smaller than
303 the inverse of the number of randomizations.



304

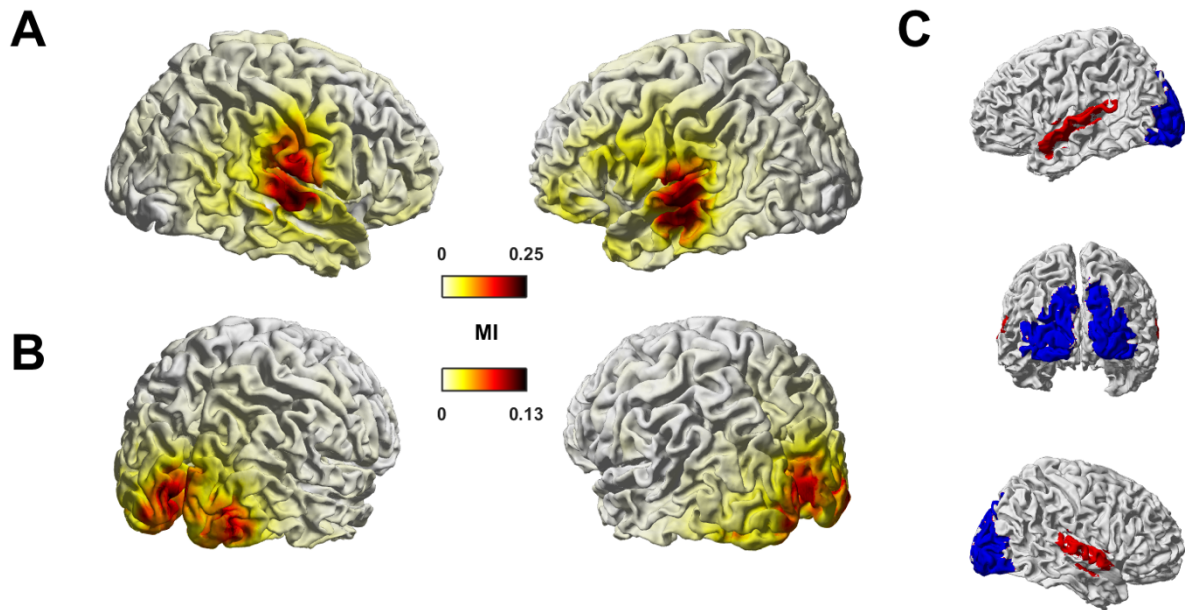
305 **Fig. 1. Stimulus material and experimental methodology.** Acoustic and visual features were extracted from audiovisual
 306 speech material and were used to quantify their cerebral tracking during audio-only and visual-only presentations. (A)
 307 The stimulus material consisted of 180 audiovisual recordings of a trained actor speaking individual matrix-style English
 308 sentences. From video recordings we extracted three features describing the dynamics of the lip aperture: the area of lip
 309 opening (lip area), its slope (lip slope), and the width of lip opening (lip width); collectively termed 'LipFeat'. The top row
 310 depicts three video frames illustrating the lip contour. From the audio waveform we extracted three acoustic features:
 311 the broadband envelope (aud env), its slope (aud slope), and a measure of dominant pitch (aud pitch); collectively termed
 312 'AudFeat'. (B) Trial-averaged percent correctly (PC) reported target words in auditory (A-only) and visual-only (V-only)
 313 conditions, with dots representing individual participants. (C) Logarithmic power spectra for individual stimulus features.
 314 For reference, a 1/f spectrum is shown as a dashed grey line. (D) Coherence between pairs of features averaged within
 315 two predefined frequency bands (0.5 - 1 Hz left; 1 - 3 Hz right, see Methods for details).

316 3. Results

317 3.1 Acoustic and visual features are tracked in temporal and occipital cortices

318 Participants were presented with either spoken speech (A-only trials) or a silent video of the speaking face
 319 (V-only trials) and were asked to report a target word for each sentence in a 4-choice comprehension task.
 320 Previous work has shown that in this dataset temporal and occipital brain regions reflect auditory and visual
 321 speech signals respectively (Keitel et al., 2020). We extend this observation to the entire group of acoustic
 322 (AudFeat) or lip features (LipFeat) using a mutual information (MI) approach (Fig. 2). The whole-brain maps
 323 demonstrate the expected prevalence of acoustic (visual) tracking in temporal (occipital) regions. Given that

324 our main questions concerned the tracking of features specifically in occipital and temporal brain regions, we
325 focused the subsequent work on atlas-based regions of interest (Fig. 2; red and blue shaded areas).



326

327 **Fig. 2. Tracking of auditory and visual features in MEG source space.** The figure shows group-level median MI values
328 for auditory (AudFeat; panel A) and lip features (LipFeat; panel B) in the frequency range from 0.5 - 8 Hz ($n = 18$
329 participants). (C) Colored shading indicates regions of interest: temporal regions in red include Brodmann area 41/42,
330 caudal area 22 (A22c), rostral area 22 (A22r) and TE1.0 and TE1.2; occipital regions in blue include middle occipital gyrus
331 (mOccG), occipital polar gyrus (OPC), inferior occipital gyrus (iOccG) and medial superior occipital gyrus (msOccG).

332 3.2 Temporal and occipital cortex represent acoustic speech features during silent lip reading

333 To address the main questions of whether temporal and occipital cortices represent auditory and visual
334 speech features during lip reading, we performed a comprehensive analysis of the tracking of both features
335 across a range of frequency bands during auditory (A-only) and visual (V-only) conditions (MI values; Figure
336 3). Importantly, to determine whether the tracking of each feature group is possibly redundant with the
337 tracking of the respective other feature group, we derived conditional MI values for each feature group,
338 obtained by partialling out the respective other group (CMI values). By comparing MI and CMI values we can
339 test, for example, whether the temporal ROI tracks the unheard speech envelope during silent lip reading
340 also when discounting for the actually presented lip trajectory. In the following we discuss the results per
341 sensory modality and region of interest.

342 As expected, when listening to speech (A-only), the temporal ROIs significantly track auditory features
343 (AudFeat) in all frequency bands tested (Fig. 3, top row, red MI data; non-parametric randomization test, all
344 bands: $p < 5 \times 10^{-5}$). This tracking persists when discounting potential contributions of the not-seen visual
345 features (red CMI data all individually significant: $p < 5 \times 10^{-5}$), though in some bands the CMI values were

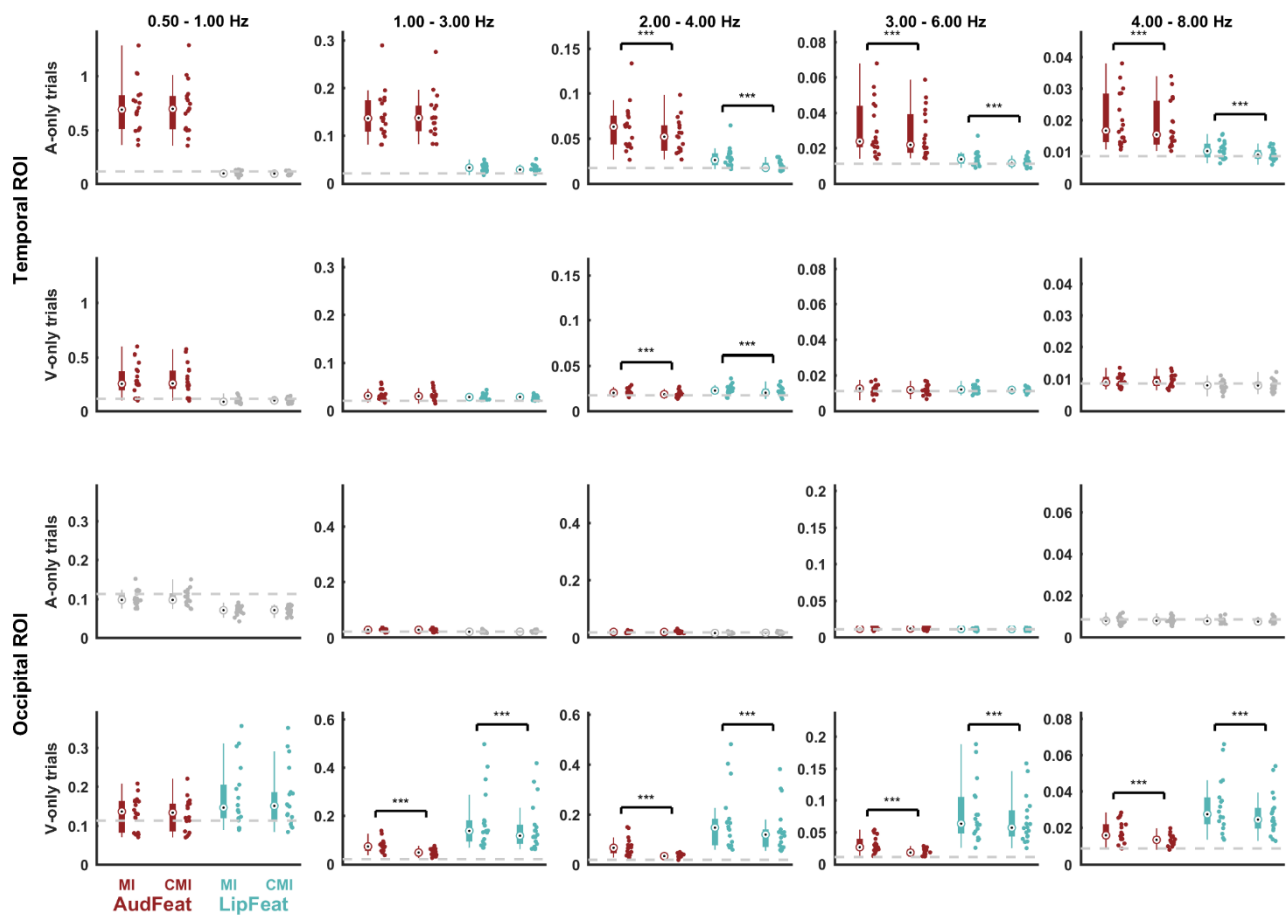
346 significantly lower than the unconditional MI (Wilcoxon signed rank test comparing MI vs. CMI, 2 - 4 Hz: Z =
347 3.59, 3 - 6 Hz: Z = 3.68, 4 - 8 Hz: Z = 3.42, all comparisons: $p < 2 \times 10^{-5}$). During the same auditory trials, lip
348 features are only marginally reflected in the temporal ROI, as shown by low but significant MI and CMI values
349 above 1Hz (Fig. 3, top row, blue MI and CMI data; all bands above 1 Hz: $p < 5 \times 10^{-5}$). This tracking of visual
350 features was significantly reduced when partialling out the physically presented auditory features (2 - 4 Hz:
351 Z = 3.59, 3 - 6 Hz: Z = 3.68, 4 - 8 Hz: Z = 3.42, all comparisons: $p < 2 \times 10^{-5}$).

352 During lip reading (V-only), the temporal ROI tracks the unheard auditory features, particularly below 1 Hz
353 (Fig. 3, 2nd row, red MI data; all bands: $p < 5 \times 10^{-5}$). Except in the 2 - 4 Hz range, the temporal ROI tracks the
354 unheard AudFeat to a similar degree as when discounting the actually presented visual signal (significant red
355 CMI values, all bands: $p < 5 \times 10^{-5}$): there were no significant differences between MI and CMI values except
356 one band (2 - 4 Hz: Z = 3.42, $p < 1 \times 10^{-4}$, see asterisks). The physically presented lip movements during these
357 V-only trials were also tracked significantly in the temporal ROI (Fig. 3, 2nd row; cyan MI and CMI data, 1 - 6
358 Hz: $p < 5 \times 10^{-5}$) but the CMI values were only marginally above chance level, suggesting that genuine visual
359 representations in temporal regions are weak.

360 As expected, during lip reading (V-only) the occipital ROI tracks lip features (LipFeat) across frequency bands
361 (Fig. 3, bottom row, cyan MI values; all bands: $p < 5 \times 10^{-5}$). Again, this tracking persists after partialling out
362 the non-presented acoustic features (cyan CMI values; all bands: $p < 5 \times 10^{-5}$), although the CMI values were
363 significantly lower than the MI (all bands above 1 Hz: $Z \geq 3.72$, $p < 2 \times 10^{-5}$). This indicates some redundancy
364 between the tracking of the physically present lip trajectory and that of the unheard auditory features.
365 Confirming this, occipital tracking of the physically presented lip signals emerges in parallel with that of the
366 non-presented auditory features (Fig. 3, bottom panel, red MI data; all bands: $p < 5 \times 10^{-5}$). This occipital
367 tracking of unheard auditory features was significantly reduced when partialling out the lip signal (MI vs. CMI
368 data; all bands above 1 Hz: $Z \geq 3.72$, $p < 2 \times 10^{-5}$) but remained statistically significant (red CMI data; all bands:
369 $p < 5 \times 10^{-5}$).

370 Finally, when listening to speech (A-only), the occipital ROI shows significant but weak tracking of auditory
371 (Fig. 3, 3rd row, red MI data; 1 - 6 Hz: $p < 5 \times 10^{-5}$) and visual features (cyan MI data; only 3 - 6 Hz: $p < 5 \times$
372 10^{-5}), suggesting that purely acoustic signals have a weak influence on occipital brain regions.

373 Collectively, these results show the expected representations of auditory features in temporal cortex during
374 listening to speech and of lip features in occipital cortex during lip reading. In addition, they reveal that during
375 lip reading, both temporal and occipital regions represent unheard auditory features and do so
376 independently of co-existing representations of the physically presented lip movements. In the auditory
377 cortex this 'restoration' of auditory signals prevails in the low delta band (0.5 - 1 Hz), in the visual cortex this
378 emerges in multiple bands.



379

380 **Fig. 3. Feature tracking across regions of interest and conditions.** For both conditions (A-only and V-only) and ROIs
 381 (temporal and occipital) the figure illustrates the strength of feature tracking for presented and physically not-present
 382 features (MI values) and the respective strength of tracking after partialling out the respective other feature group (CMI
 383 values). Each panel depicts (from left to right) the MI for AudFeat, the CMI for AudFeat partialling out LipFeat, the MI for
 384 LipFeat, and the CMI for LipFeat partialling out AudFeat. Dots represent individual participants ($n = 18$). Bars indicate
 385 the median, 25th and 75th percentile. The grey dashed line indicates the 99th percentile of the frequency-specific
 386 randomized maximum distribution correcting for all other dimensions. Conditions below a group-level significance
 387 threshold of 0.01 are greyed out. Brackets with asterisks indicate significant differences between MI and CMI values,
 388 based on a Wilcoxon signed-rank test (* $p < 0.01$, ** $p < 0.005$, *** $p < 0.001$). Units for MI and CMI are in bits.

389 To obtain an estimate of the effect size of the restoration of the unheard AudFeat during lip reading we
 390 expressed these CMI values relative to those of the tracking of the respectively modality-preferred inputs of
 391 each ROI (Fig. 4A): for temporal regions the tracking of AudFeat during A-only trials and for occipital regions
 392 the tracking of LipFeat during V-only trials. In the temporal ROI, the restoration effect size, i.e. the tracking
 393 of AudFeat during lip reading, was about a third as strong as this feature's tracking while directly listening to
 394 speech (Fig. 4A; top row; $\text{AudFeat}_{\text{V-only}} / \text{AudFeat}_{\text{A-only}}$; 0.5 - 1 Hz: median = 0.37, 1 - 3 Hz: median = 0.24). In
 395 the occipital ROI, the tracking of AudFeat was about half as strong or stronger compared to the tracking of
 396 lip features when seeing the speaker (Fig. 4A; bottom row; $\text{AudFeat}_{\text{V-only}} / \text{LipFeat}_{\text{V-only}}$; 0.5 - 1 Hz: median =
 397 0.84, 1 - 3 Hz: median = 0.4). Albeit smaller than the tracking of the respective modality-preferred sensory

398 inputs, the restoration of unheard auditory features still results in a prominent signature in temporally
399 aligned brain activity in both cortices.

400 3.3 Feature tracking is bilateral and prevails across anatomical brain areas

401 Having established the tracking of auditory and lip features in both temporal and occipital ROIs, we probed
402 whether this tracking is possibly lateralized in a statistical sense and whether it potentially differs among the
403 anatomical areas grouped into temporal and occipital ROIs respectively. For this analysis we focused on the
404 conditional tracking of each feature group. Comparing CMI values among anatomical areas (averaged across
405 hemispheres) for each ROI (occipital, temporal), frequency band (0.5 - 1 and 1 - 3 Hz), condition and feature
406 group revealed a significant effect of area for AudFeat tracking in the temporal ROI during A-only trials (Table
407 1; 0.5 - 1 Hz: $\chi^2(3) = 27.02$, $p = 4.7 \times 10^{-6}$, $\epsilon^2 = 0.35$; 1 - 3 Hz: $\chi^2(3) = 29.62$, $p = 2.7 \times 10^{-6}$, $\epsilon^2 = 0.39$; p-values
408 FDR-corrected). Post hoc comparisons revealed that in both bands, tracking of AudFeat was higher in A41/42
409 and A22c compared to TE1.0/1.2 and A22r (Tukey-Kramer test, all tests $p < 10^{-5}$). The effect of Area was close
410 to but not significant for LipFeat tracking in the occipital ROI during V-only trials (0.5 - 1 Hz: $\chi^2(3) = 12.3$, $p =$
411 0.026 , $\epsilon^2 = 0.14$; 1 - 3 Hz: $\chi^2(3) = 14.57$, $p = 0.012$, $\epsilon^2 = 0.17$). Importantly, these results suggest that while the
412 tracking of auditory features was stronger in the early auditory regions during A-only trials, the restoration
413 of unheard auditory features during lip reading emerges to a similar degree among the individual temporal
414 and occipital areas.

415 We performed a similar analysis comparing the CMI values within temporal or occipital ROIs between
416 hemispheres. This revealed no significant effects of hemispheres (Table 2), hence offering no evidence for a
417 statistical lateralization of feature tracking in the present data.

| ROI | Anatomical area | 0.5 - 1 Hz | | | | 1 - 3 Hz | | | |
|----------------------|-----------------|------------|----------------------------|--------|-------------|----------|----------------------------|--------|-------------|
| | | AudCMI | Chisq; pval | LipCMI | Chisq; pval | AudCMI | Chisq; pval | LipCMI | Chisq; pval |
| A-only trials | | | | | | | | | |
| AC | A41/42 | 0.97 | 27.02 ; 4.7e-05 | 0.096 | 2.47 ; 0.59 | 0.19 | 29.62 ; 2.7e-05 | 0.032 | 5.14 ; 0.32 |
| | TE1.0/1.2 | 0.56 | | 0.099 | | 0.11 | | 0.028 | |
| | A22c | 0.86 | | 0.098 | | 0.18 | | 0.033 | |
| | A22r | 0.5 | | 0.093 | | 0.095 | | 0.029 | |
| VC | mOccG | 0.1 | 3.50 ; 0.47 | 0.073 | 0.66 ; 0.88 | 0.025 | 2.71 ; 0.58 | 0.02 | 1.97 ; 0.66 |
| | OPC | 0.09 | | 0.069 | | 0.025 | | 0.02 | |
| | iOccG | 0.11 | | 0.068 | | 0.027 | | 0.021 | |
| | msOccG | 0.11 | | 0.074 | | 0.029 | | 0.021 | |
| V-only trials | | | | | | | | | |
| AC | A41/42 | 0.33 | 4.59 ; 0.36 | 0.1 | 5.14 ; 0.32 | 0.034 | 5.24 ; 0.32 | 0.027 | 1.00 ; 0.85 |
| | TE1.0/1.2 | 0.25 | | 0.088 | | 0.031 | | 0.028 | |

| | | | | | | | | | |
|-----------|--------|------|-------------|-------|---------------|-------|-------------|-------|---------------|
| | A22c | 0.34 | | 0.1 | | 0.035 | | 0.027 | |
| | A22r | 0.22 | | 0.085 | | 0.028 | | 0.029 | |
| VC | mOccG | 0.13 | 3.90 ; 0.44 | 0.17 | 12.30 ; 0.026 | 0.045 | 8.20 ; 0.13 | 0.15 | 14.57 ; 0.012 |
| | OPC | 0.14 | | 0.19 | | 0.06 | | 0.2 | |
| | iOccG | 0.14 | | 0.2 | | 0.048 | | 0.17 | |
| | msOccG | 0.11 | | 0.11 | | 0.039 | | 0.082 | |

418

419 **Table 1. Feature tracking in individual anatomical areas within temporal and occipital ROIs.** The table lists
 420 CMI values and a statistical comparison between the individual atlas-defined areas (Kruskal-Wallis tests,
 421 reporting chi-squares and p-values). Bold numbers indicate statistically significant results. P-values are FDR-
 422 corrected within this Table.

| | | 0.5 - 1 Hz | | | | 1 - 3 Hz | | | |
|----------------------|------------|------------|--------------|--------|---------------|----------|--------------|--------|--------------|
| ROI | Hemisphere | AudCMI | Z; pval | LipCMI | Z; pval | AudCMI | Z; pval | LipCMI | Z; pval |
| A-only trials | | | | | | | | | |
| AC | left | 0.8 | 1.20 ; 0.59 | 0.094 | -0.33 ; 0.74 | 0.13 | -0.81 ; 0.59 | 0.028 | -1.11 ; 0.59 |
| | right | 0.64 | | 0.099 | | 0.15 | | 0.031 | |
| VC | left | 0.1 | -0.37 ; 0.74 | 0.07 | -0.33 ; 0.74 | 0.027 | 0.81 ; 0.59 | 0.021 | 0.63 ; 0.65 |
| | right | 0.1 | | 0.072 | | 0.025 | | 0.02 | |
| V-only trials | | | | | | | | | |
| AC | left | 0.31 | 0.89 ; 0.59 | 0.098 | 0.76 ; 0.59 | 0.035 | 0.85 ; 0.59 | 0.025 | -1.85 ; 0.26 |
| | right | 0.26 | | 0.091 | | 0.03 | | 0.03 | |
| VC | left | 0.11 | -2.24 ; 0.2 | 0.14 | -2.98 ; 0.046 | 0.043 | -1.68 ; 0.3 | 0.13 | -2.07 ; 0.21 |
| | right | 0.15 | | 0.2 | | 0.054 | | 0.18 | |

423

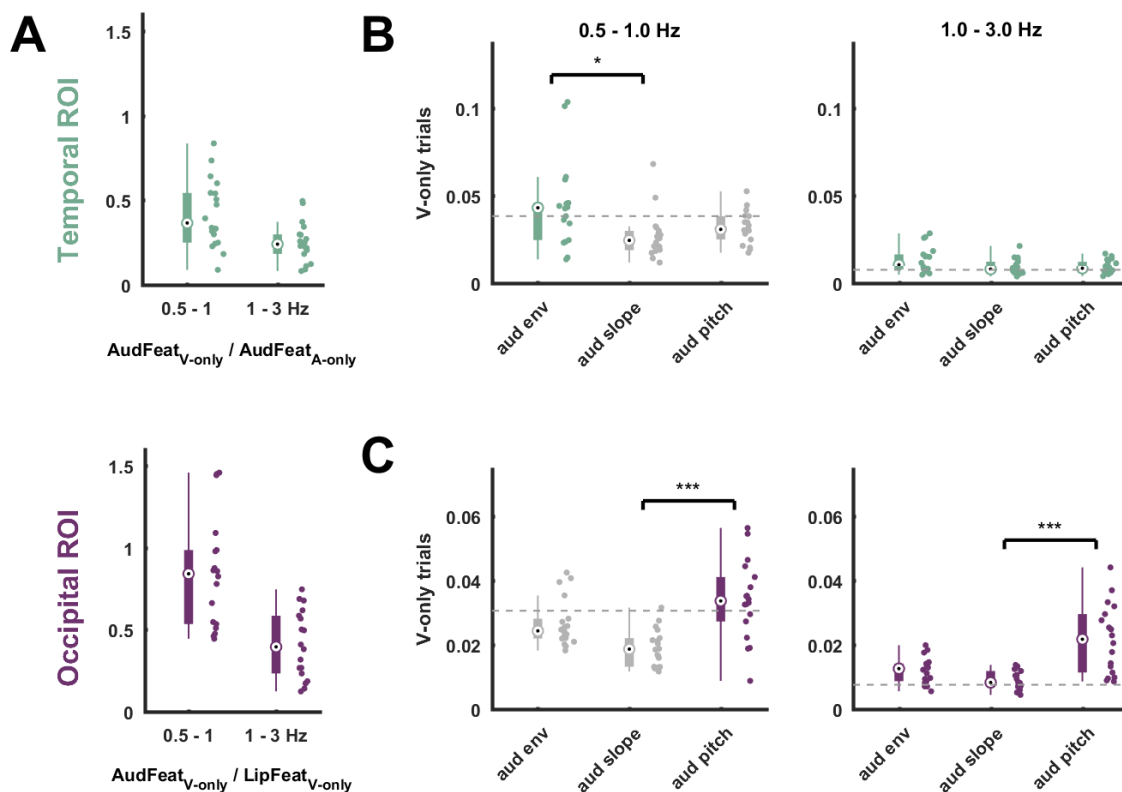
424 **Tab. 2. Feature tracking in each hemisphere.** The table lists CMI values and a statistical comparison between
 425 hemispheres (Kruskal-Wallis tests, reporting chi-squares and p-values). P-values are FDR-corrected within this
 426 Table.

427 3.4 Occipital cortex reflects pitch more than other acoustic features during lipreading

428 Having established that occipital and temporal regions track unheard auditory features, we then asked how
 429 individual features contribute to these representations. For this we focused on the key condition of interest:
 430 the tracking of AudFeat in the delta range in V-only trials (Fig. 4 B,C). We quantified the CMI for each
 431 individual feature, while discounting the evidence about all other left-out visual and auditory features, hence
 432 focusing on the unique tracking of each individual acoustic feature.

433 For the temporal ROI this revealed the prominent tracking of aud env (Fig. 4B). In the in the 0.5 - 1 Hz band
434 only the CMI for aud env was above chance ($p < 5 \times 10^{-5}$) and there was a significant effect of feature (Kruskal-
435 Wallis rank test $\chi^2(2) = 9.27$, $p = 9.1 \times 10^{-4}$, $\epsilon^2 = 0.14$). Post-hoc tests revealed that the CMI for aud env differed
436 significantly from that of aud slope (Tukey-Kramer test, $p = 6.2 \times 10^{-4}$; the other comparisons were not
437 significant; $p = 0.35$ for env vs. slope and $p = 0.22$ for slope vs. pitch). In the 1 - 3 Hz band, the tracking of all
438 auditory features was significant (all features: $p < 5 \times 10^{-5}$) and there was no significant effect of features
439 ($\chi^2(2) = 4.14$, $p = 0.13$, $\epsilon^2 = 0.04$).

440 For the occipital ROI, this revealed a dominance of aud pitch (Fig. 4C). In the 0.5 - 1 Hz band, only the CMI of
441 aud pitch was above chance ($p < 5 \times 10^{-5}$), a direct comparison revealed a significant effect of features (0.5 -
442 1 Hz: $\chi^2(2) = 18.28$, $p = 1.07 \times 10^{-4}$, $\epsilon^2 = 0.32$) and post-hoc tests revealed a significant difference between aud
443 pitch and aud slope ($p = 7.03 \times 10^{-5}$), while the other comparisons were not significant ($p = 0.26$ for pitch vs.
444 env and $p = 0.02$ for env vs. slope). In the 1 - 3 Hz range, the tracking of all features was significant (all features:
445 $p < 5 \times 10^{-5}$), there was a significant effect of features $\chi^2(2) = 19.2$, $p = 6.77 \times 10^{-5}$, $\epsilon^2 = 0.34$), and post-hoc
446 tests revealed a significant difference between pitch and slope ($p = 3.61 \times 10^{-5}$), while the other comparisons
447 were not significant ($p = 0.05$ for pitch vs. env and $p = 0.12$ for env vs. slope). Collectively these results suggest
448 that the restoration of acoustic information in occipital regions emphasizes spectral features, while in
449 temporal regions this emphasizes the temporal speech envelope.



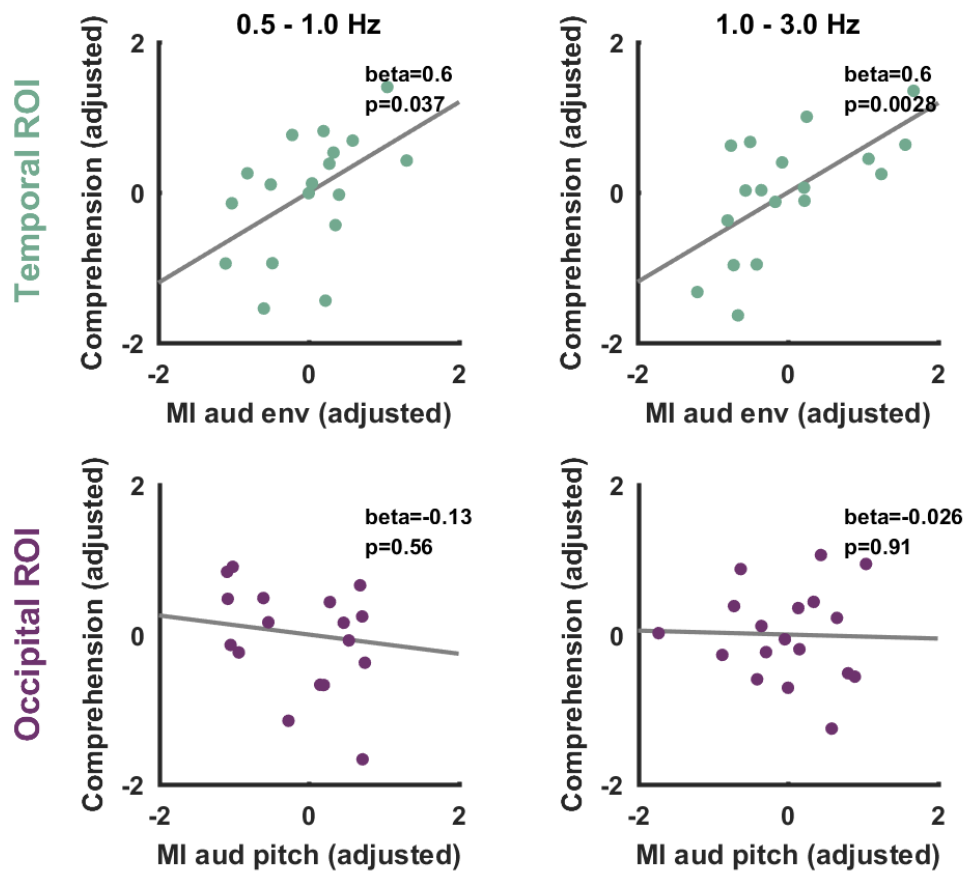
450
451 **Fig. 4. Modality dominance and tracking of individual auditory features during lip reading.** (A) Comparison of the
452 tracking of unheard AudFeat over the tracking of the modality-preferred sensory input in each ROI (i.e. AudFeat during

453 *A-only trials in the temporal ROI; LipFeat during V-only trials in the occipital ROI). (B,C) Tracking of individual auditory*
454 *features during V-only trials conditioned on all other auditory and lip features in temporal (B) and occipital (C) ROIs.*
455 *Brackets with asterisks indicate levels of significance from one-way Kruskal-Wallis rank test with post-hoc Tukey-Kramer*
456 *testing (* $p < 0.01$, ** $p < 0.005$, *** $p < 0.001$). Dots represent individual data points. Bars indicate the median, 25th*
457 *and 75th percentile. The grey dashed line indicates the 99th percentile of the frequency-specific randomized maximum*
458 *distribution correction for all other features. Units in (A) are a ratio, in panels (B) and (C) units are in bits.*

459 **3.5 Tracking of auditory features is associated with lip reading performance**

460 Finally, we probed the relevance of the restoration of unheard auditory features during silent lip reading for
461 comprehension. For this we probed the predictive power of the MI about specific auditory features in either
462 ROI for comprehension performance during V-only trials (Fig. 5). We specifically focused on the tracking of
463 aud env in the temporal ROI and of aud pitch in the occipital ROI as the dominant feature-specific
464 representations (c.f. Fig. 4B,C). Using linear models we predicted comprehension scores across participants
465 based on the tracking indices of interest and while discounting for potential confounds from differences in
466 signal-to-noise ratio.

467 The results show that variations in comprehension scores are well predicted by the collective measures of
468 feature tracking (0.5 - 1 Hz: $R^2 = 0.74$, 1 - 3 Hz: $R^2 = 0.8$). Importantly, the tracking of aud env in the temporal
469 ROI was significantly predictive of lip reading performance (0.5 - 1 Hz: $\beta = 0.6$, $p = 0.037$; 1 - 3 Hz: aud env β
470 $= 0.6$, $p = 2.8 \times 10^{-4}$), while tracking of pitch in the occipital ROI was not (0.5 - 1 Hz: $\beta = -0.13$, $p = 0.56$; 1 - 3
471 Hz: $\beta = -0.026$, $p = 0.91$). This conclusion is also supported by Bayes factors for the added predictive power of
472 aud env and aud pitch to these models (aud env in the temporal ROI; 0.5 - 1 Hz: BF = 3.12; 1 - 3 Hz: BF = 26.34;
473 aud pitch in the occipital ROI; 0.5 - 1 Hz BF = 0.3; 1 - 3 Hz BF = 0.24).



474

475

476

477

478

479

Fig. 5. Association between lip reading performance and tracking of auditory features. Across participants the tracking of aud env during V-only trials in the temporal ROI but not the tracking of aud pitch in the occipital ROI was significantly associated with comprehension performance (PC) across participants in visual trials. Graphs show partial residual plots, dots represent individual data points and the line indicates the linear fit to the target variable from the full regression model.

480

4. Discussion

481

482

483

484

485

486

487

488

489

490

491

Natural face-to-face speech is intrinsically multidimensional and provides the auditory and visual pathways with partly distinct acoustic and visual information. These pathways could in principle focus mainly on the processing of their modality-specific signals, effectively keeping the two input modalities largely separated. Yet, many studies highlight the intricate multisensory nature of speech-related representations in the brain, including multisensory convergence at early stages of the hierarchy (Bernstein and Liebenthal, 2014; Crosse et al., 2015; Schroeder et al., 2008; Schroeder and Lakatos, 2009) as well as in classically amodal speech regions (Keitel et al., 2020; Mégevand et al., 2020; Scott, 2019). However, as the present results point out, the auditory and visual pathways are also capable of ‘restoring’ information about an absent modality-specific speech component. While seeing a silent speaker, both auditory and visual cortices track the temporal dynamics of the speech envelope and spectral features respectively, in a manner that is independent on the physically presented lip movements. Importantly, these ‘restored’ representations of

492 acoustic speech features relate to participants' comprehension, suggesting that they may form a central
493 component of silent lip reading.

494 **4.1 Auditory and visual cortex reflect acoustic speech features during lip reading**

495 We systematically quantified the tracking of auditory and visual speech features during unisensory auditory
496 and visual (lip reading) conditions in dynamically entrained brain activity. As expected, this analysis confirmed
497 that early auditory and visual regions reflect acoustic and visual signals respectively at the time scales of delta
498 (< 4 Hz) and theta (4 - 8 Hz) band activity, in line with a large body of previous work (Aiken and Picton, 2008;
499 Bauer et al., 2020; Doelling et al., 2014; Giraud and Poeppel, 2012; Haegens and Zion Golumbic, 2018; Obleser
500 and Kayser, 2019). In addition, we found that during lip reading both regions contained significant
501 information about the unheard auditory features, also when discounting for the physically presented lip
502 movements. This representation of acoustic features prevailed in the low delta band in auditory and the delta
503 and theta bands in the visual cortex. Interestingly, this representation emphasized the temporal speech
504 envelope in auditory cortex and spectral features (i.e. pitch) in the visual cortex. These results not only
505 support that both regions are active during lip reading (Besle et al., 2008; Calvert et al., 1997; Calvert and
506 Campbell, 2003; Ludman et al., 2000; Luo et al., 2010), but directly show that they contain temporally and
507 feature-specific representations derived from lip movements that are also relevant for comprehension.

508 These results advance our understanding of how the brain exploits lip movements for speech-related
509 processes in a number of ways. The restoration of auditory features during silent lip reading had been
510 suggested in two previous studies, one showing the coherence of temporal brain activity with the non-
511 presented speech envelope (Bourguignon et al., 2020) and another showing the coherence between occipital
512 activity and the envelope (Hauswald et al., 2018; Suess et al., 2022). Yet, these studies differed in their precise
513 experimental designs, their statistical procedures revealing the 'restoration' effect, and did not probe a direct
514 link to comprehension performance. The present data demonstrate that such tracking of auditory speech-
515 derived features indeed emerges in parallel and in the same participants, and, importantly, predicts
516 comprehension. This suggests that perceptually relevant and possibly linked mechanisms may underlie the
517 simultaneous processing of visual speech along visual and auditory pathways. In addition, our data show that
518 this restoration emerges across a wider range of time scales as reported before (Bourguignon et al., 2020),
519 and also when discounting for the physically present lip signals. The latter is particularly important, as the
520 mere coherence of dynamic brain activity with the acoustic speech envelope may otherwise simply reflect
521 those aspects of the physically-present visual speech that is directly redundant with the acoustic domain
522 (Daube et al., 2019). Finally, our data suggest that this restoration is largely bilateral and emerges across a
523 number of anatomically-identified areas, suggesting that it forms a generic property of the respective
524 pathways.

525 Based on the same dataset as analyzed here, we recently showed that the identity of task-relevant words
526 can be classified from the activity in multiple brain regions during lip reading and listening to speech (Keitel

527 et al., 2020). While this previous study suggested that lip reading is facilitated by processes in early visual
528 regions, the respective analysis focused on lexical identity and did not consider the individual features that
529 may carry or contribute to such lexical information. The present results hence complement our previous work
530 by demonstrating the alignment of temporal and occipital activity to the dynamics of the lip contour and
531 specific acoustic features.

532 **4.2 Lip reading activates a network of occipital and temporal regions**

533 Previous work has shown that lip movements activate a network of temporal, parietal and frontal regions
534 (Bourguignon et al., 2020; Calvert et al., 1997; Capek et al., 2008; O’Sullivan et al., 2017; Ozker et al., 2018;
535 Paulesu et al., 2003; Pekkola et al., 2005) and that both occipital and motor regions can align their activity to
536 the dynamics of lip movements (Park et al., 2018, 2016). The present data substantiate this, but also show
537 that the representation of the physically visible lip trajectory along visual pathways is accompanied by the
538 representation of spectral acoustic features, a type of selectivity not directly revealed previously (Suess et
539 al., 2022). Spectral features are vital for a variety of listening tasks (Albouy et al., 2020; Bröhl and Kayser,
540 2020; Ding and Simon, 2013; Tivadar et al., 2020, 2018), and oro-facial movements provide concise
541 information about the spectral domain. Importantly, as shown recently, seeing the speaker’s mouth allows
542 discriminating formant frequencies and provides a comprehension benefit particularly when spectral speech
543 features are degraded (Plass et al., 2020). This suggests a direct and comprehension-relevant link between
544 the dynamics of the lip contour and spectral speech features (Campbell, 2008). Hence, a representation of
545 acoustic features during silent lip reading may underlie the mapping of lip movements onto phonological
546 units such as visemes, a form of language-specific representation emerging along visual pathways (Nidiffer
547 et al., 2021; O’Sullivan et al., 2017).

548 Our results corroborate the notion that multisensory speech reception is not contingent only on high-level
549 and modality-neutral representations. Rather, they suggest that cross-modal correspondences between
550 auditory and visual speech exist along a number of dimensions, including basic temporal properties (Bizley
551 et al., 2016; Chandrasekaran et al., 2009) as well as mid-level features, such as pitch or visual object features,
552 whose representation is traditionally considered to be modality specific (Crosse et al., 2015; Plass et al., 2020;
553 Schroeder et al., 2008; Zion Golumbic et al., 2013). Previous work has debated whether visual speech is
554 mainly encoded along the auditory pathways or whether occipital regions contribute genuine speech-specific
555 representations (O’Sullivan et al., 2017; Ozker et al., 2018). Our results speak in favor of occipital regions
556 supporting speech reception by establishing multiple forms of speech-related information, including those
557 aligned with the acoustic domain revealed here, and those establishing visemic categories based on
558 complementary visual signals (Nidiffer et al., 2021; Suess et al., 2022). Which precise occipital areas and by
559 which patterns of connectivity they contribute to comprehension remains to be investigated, but both kinds
560 of representations may well emerge from distinct temporal-occipital networks (Bernstein and Liebenthal,
561 2014). While visemic information may be driven by object-related lateral occipital regions, the more auditory-

562 aligned representations such as the restoration of spectral signatures may be directly driven by the
563 connectivity between occipital areas and superior temporal regions, which play a key role for audio-visual
564 speech integration (Arnal et al., 2009; Lazard and Giraud, 2017).

565 In the auditory cortex, the alignment of neural activity to the unheard speech envelope may reflect the
566 predictive influence of visual signals on guiding the excitability of auditory pathways via low frequency
567 oscillations (Schroeder et al., 2008). This alignment of auditory cortical activity to attended or expected
568 sounds is well documented and has been proposed as a cornerstone of multisensory speech integration in
569 general (Lakatos et al., 2008; Schroeder and Lakatos, 2009; Stefanics et al., 2010). One hypothesis is that this
570 alignment may facilitate the segmentation or parsing of the speech stream (Ding et al., 2016; Giraud and
571 Poeppel, 2012; Meyer et al., 2017). In this light the restoration of the speech envelope during lip reading
572 suggests that such segmentation processes along the auditory pathways align to the presumed or expected
573 acoustic counterpart underlying the received visual signal. This process would then act in parallel to visemic
574 analysis in the visual pathway, and imply central functions of both auditory and visual pathways in lip reading.

575 **5. Conclusion**

576 Lip reading induces representations of the dynamic lip contour along visual pathways. Our results show that
577 the brain derives representations of acoustic speech features from this sensory input as well, reflecting a
578 form of restoration of acoustic speech-related features in auditory and visual cortices. In the auditory cortex
579 these restored representations are predictive of lip reading performance, suggesting that they may form a
580 central component of multisensory comprehension benefits.

581 **Credit author statement**

582 Conceptualization: A.K., C.K., Project administration: A.K., C.K., Funding acquisition: C.K., Methodology: F.B.,
583 A.K., C.K., Software: F.B., A.K., Formal Analysis: F.B., Investigation: F.B., Data Curation: F.B., Supervision: C.K.,
584 Writing Original Draft: F.B., C.K., Writing Review & Editing: F.B., A.K., C.K.

585 **Data and code availability**

586 Data and code used in this study are publicly available on the Data Server of the University of Bielefeld
587 (<https://gitlab.ub.uni-bielefeld.de/felix.broehl/fb02>).

588 **Declaration of competing interest**

589 We declare no conflict of interest.

590 **Acknowledgement**

591 This work was supported by the UK Biotechnology and Biological Sciences Research Council (BBSRC,
592 BB/L027534/1) and the European Research Council (ERC-2014-CoG; grant No 646657)

593

594 References

- 595 Aiken, S.J., Picton, T.W., 2008. Human cortical responses to the speech envelope. *Ear Hear.* 29, 139–157.
596 <https://doi.org/10.1097/AUD.0b013e31816453dc>
- 597 Albouy, P., Benjamin, L., Morillon, B., Zatorre, R.J., 2020. Distinct sensitivity to spectrotemporal modulation
598 supports brain asymmetry for speech and melody. *Science (80-.)*. 367, 1043–1047.
599 <https://doi.org/10.1126/science.aaz3468>
- 600 Arnal, L.H., Morillon, B., Kell, C.A., Giraud, A.L., 2009. Dual neural routing of visual facilitation in speech
601 processing. *J. Neurosci.* 29, 13445–13453. <https://doi.org/10.1523/JNEUROSCI.3194-09.2009>
- 602 Bauer, A.K.R., Debener, S., Nobre, A.C., 2020. Synchronisation of Neural Oscillations and Cross-modal
603 Influences. *Trends Cogn. Sci.* <https://doi.org/10.1016/j.tics.2020.03.003>
- 604 Benjamini, Y., Hochberg, Y., 1995. Controlling the False Discovery Rate: A Practical and Powerful Approach
605 to Multiple Testing. *J. R. Stat. Soc. Ser. B.*
- 606 Bernstein, L.E., Auer, E.T., Moore, J.K., Ponton, C.W., Don, M., Singh, M., 2002. Visual speech perception
607 without primary auditory cortex activation. *Neuroreport* 13, 311–315.
608 <https://doi.org/10.1097/00001756-200203040-00013>
- 609 Bernstein, L.E., Jiang, J., Pantazis, D., Lu, Z.-L., Joshi, A., 2011. Visual phonetic processing localized using
610 speech and nonspeech face gestures in video and point-light displays. *Hum. Brain Mapp.* 32, 1660–
611 1676. <https://doi.org/10.1002/hbm.21139>
- 612 Bernstein, L.E., Liebenthal, E., 2014. Neural pathways for visual speech perception. *Front. Neurosci.*
613 <https://doi.org/10.3389/fnins.2014.00386>
- 614 Besle, J., Fischer, C., Bidet-Caulet, A., Lecaigard, F., Bertrand, O., Giard, M.H., 2008. Visual activation and
615 audiovisual interactions in the auditory cortex during speech perception: Intracranial recordings in
616 humans. *J. Neurosci.* 28, 14301–14310. <https://doi.org/10.1523/JNEUROSCI.2875-08.2008>
- 617 Bizley, J.K., Maddox, R.K., Lee, A.K.C., 2016. Defining Auditory-Visual Objects: Behavioral Tests and
618 Physiological Mechanisms. *Trends Neurosci.* 39, 74–85. <https://doi.org/10.1016/j.tins.2015.12.007>
- 619 Boersma, P., van Heuven, V., 2001. PRAAT, a system for doing phonetics by computer. *Glott Int.* 5, 341–347.
- 620 Bourguignon, M., Baart, M., Kapnoula, E.C., Molinaro, N., 2020. Lip-reading enables the brain to synthesize
621 auditory features of unknown silent speech. *J. Neurosci.* 40, 1053–1065.
622 <https://doi.org/10.1523/JNEUROSCI.1101-19.2019>
- 623 Brodbeck, C., Simon, J.Z., 2020. Continuous speech processing. *Curr. Opin. Physiol.* 18, 25–31.
624 <https://doi.org/10.1016/j.cophys.2020.07.014>
- 625 Bröhl, F., Kayser, C., 2020. Delta/theta band EEG differentially tracks low and high frequency speech-
626 derived envelopes. *Neuroimage* 233, 117958. <https://doi.org/10.1101/2020.07.26.221838>
- 627 Calvert, G.A., Bullmore, E.T., Brammer, M.J., Campbell, R., Williams, S.C.R., McGuire, P.K., Woodruff, P.W.R.,
628 Iversen, S.D., David, A.S., 1997. Activation of auditory cortex during silent lipreading. *Science (80-.)*.
629 276, 593–596. <https://doi.org/10.1126/science.276.5312.593>

- 630 Calvert, G.A., Campbell, R., 2003. Reading speech from still and moving faces: The neural substrates of
631 visible speech. *J. Cogn. Neurosci.* 15, 57–70. <https://doi.org/10.1162/089892903321107828>
- 632 Campbell, R., 2008. The processing of audio-visual speech: Empirical and neural bases. *Philos. Trans. R. Soc.*
633 *B Biol. Sci.* 363, 1001–1010. <https://doi.org/10.1098/rstb.2007.2155>
- 634 Capek, C.M., MacSweeney, M., Woll, B., Waters, D., McGuire, P.K., David, A.S., Brammer, M.J., Campbell, R.,
635 2008. Cortical circuits for silent speechreading in deaf and hearing people. *Neuropsychologia* 46,
636 1233–1241. <https://doi.org/10.1016/j.neuropsychologia.2007.11.026>
- 637 Chandrasekaran, C., Trubanova, A., Stillittano, S., Caplier, A., Ghazanfar, A.A., 2009. The natural statistics of
638 audiovisual speech. *PLoS Comput. Biol.* 5, e1000436. <https://doi.org/10.1371/journal.pcbi.1000436>
- 639 Crosse, M.J., Butler, J.S., Lalor, E.C., 2015. Congruent Visual Speech Enhances Cortical Entrainment to
640 Continuous Auditory Speech in Noise-Free Conditions. *J. Neurosci.* 35, 14195–204.
641 <https://doi.org/10.1523/JNEUROSCI.1829-15.2015>
- 642 Daube, C., Ince, R.A.A., Gross, J., 2019. Simple Acoustic Features Can Explain Phoneme-Based Predictions of
643 Cortical Responses to Speech. *Curr. Biol.* 29, 1924–1937.e9.
644 <https://doi.org/10.1016/j.CUB.2019.04.067>
- 645 Di Liberto, G.M., Lalor, E.C., Millman, R.E., 2018. Causal cortical dynamics of a predictive enhancement of
646 speech intelligibility. *Neuroimage* 166, 247–258. <https://doi.org/10.1016/j.neuroimage.2017.10.066>
- 647 Ding, N., Melloni, L., Zhang, H., Tian, X., Poeppel, D., 2016. Cortical tracking of hierarchical linguistic
648 structures in connected speech. *Nat. Neurosci.* 19, 158–64. <https://doi.org/10.1038/nn.4186>
- 649 Ding, N., Simon, J.Z., 2013. Adaptive temporal encoding leads to a background-insensitive cortical
650 representation of speech. *J. Neurosci.* 33, 5728–35. <https://doi.org/10.1523/JNEUROSCI.5297-12.2013>
- 651 Doelling, K.B., Arnal, L.H., Ghitza, O., Poeppel, D., 2014. Acoustic landmarks drive delta-theta oscillations to
652 enable speech comprehension by facilitating perceptual parsing. *Neuroimage* 85, 761–768.
653 <https://doi.org/10.1016/j.neuroimage.2013.06.035>
- 654 Etard, O., Reichenbach, T., 2019. Neural Speech Tracking in the Theta and in the Delta Frequency Band
655 Differentially Encode Clarity and Comprehension of Speech in Noise. *J. Neurosci.* 39, 5750–5759.
656 <https://doi.org/10.1523/JNEUROSCI.1828-18.2019>
- 657 Giordano, B.L., Ince, R.A.A., Gross, J., Schyns, P.G., Panzeri, S., Kayser, C., 2017. Contributions of local
658 speech encoding and functional connectivity to audio-visual speech perception. *Elife* 6.
659 <https://doi.org/10.7554/eLife.24763>
- 660 Giraud, A.L., Poeppel, D., 2012. Cortical oscillations and speech processing: Emerging computational
661 principles and operations. *Nat. Neurosci.* 15, 511–517. <https://doi.org/10.1038/nn.3063>
- 662 Grant, K.W., Seitz, P.-F., 2000. The use of visible speech cues for improving auditory detection of spoken
663 sentences. *J. Acoust. Soc. Am.* 108, 1197. <https://doi.org/10.1121/1.1288668>
- 664 Gross, J., Hoogenboom, N., Thut, G., Schyns, P., Panzeri, S., Belin, P., Garrod, S., 2013. Speech Rhythms and
665 Multiplexed Oscillatory Sensory Coding in the Human Brain. *PLoS Biol.* 11, e1001752.
666 <https://doi.org/10.1371/journal.pbio.1001752>

- 667 Haegens, S., Zion Golumbic, E., 2018. Rhythmic facilitation of sensory processing: A critical review.
668 *Neurosci. Biobehav. Rev.* 86, 150–165. <https://doi.org/10.1016/j.neubiorev.2017.12.002>
- 669 Hauswald, A., Lithari, C., Collignon, O., Leonardelli, E., Weisz, N., 2018. A Visual Cortical Network for
670 Deriving Phonological Information from Intelligible Lip Movements. *Curr. Biol.* 28, 1453-1459.e3.
671 <https://doi.org/10.1016/j.cub.2018.03.044>
- 672 Ince, R.A.A., Giordano, B.L., Kayser, C., Rousselet, G.A., Gross, J., Schyns, P.G., 2017. A statistical framework
673 for neuroimaging data analysis based on mutual information estimated via a gaussian copula. *Hum.*
674 *Brain Mapp.* 38, 1541–1573. <https://doi.org/10.1002/hbm.23471>
- 675 Keitel, A., Gross, J., Kayser, C., 2020. Shared and modality-specific brain regions that mediate auditory and
676 visual word comprehension. *Elife* 9, 1–23. <https://doi.org/10.7554/ELIFE.56972>
- 677 Keitel, A., Gross, J., Kayser, C., 2018. Perceptually relevant speech tracking in auditory and motor cortex
678 reflects distinct linguistic features. *PLoS Biol.* 16, e2004473.
679 <https://doi.org/10.1371/journal.pbio.2004473>
- 680 Keitel, A., Ince, R.A.A., Gross, J., Kayser, C., 2017. Auditory cortical delta-entrainment interacts with
681 oscillatory power in multiple fronto-parietal networks. *Neuroimage* 147, 32–42.
682 <https://doi.org/10.1016/j.neuroimage.2016.11.062>
- 683 Koike, K.J., Hurst, M.K., Wetmore, S.J., 1994. Correlation between the American Academy of
684 Otolaryngology-Head and Neck Surgery Five-Minute Hearing Test and standard audiologic data.
685 *Otolaryngol. - Head Neck Surg.* 111, 625–632. [https://doi.org/10.1016/S0194-5998\(94\)70531-3](https://doi.org/10.1016/S0194-5998(94)70531-3)
- 686 Lakatos, P., Karmos, G., Mehta, A.D., Ulbert, I., Schroeder, C.E., 2008. Entrainment of neuronal oscillations
687 as a mechanism of attentional selection. *Science* 320, 110–3.
688 <https://doi.org/10.1126/science.1154735>
- 689 Lazard, D.S., Giraud, A.L., 2017. Faster phonological processing and right occipito-temporal coupling in deaf
690 adults signal poor cochlear implant outcome. *Nat. Commun.* 8, 1–9.
691 <https://doi.org/10.1038/ncomms14872>
- 692 Ludman, C.N., Summerfield, A.Q., Hall, D., Elliott, M., Foster, J., Hykin, J.L., Bowtell, R., Morris, P.G., 2000.
693 Lip-reading ability and patterns of cortical activation studied using fMRI. *Br. J. Audiol.* 34, 225–230.
694 <https://doi.org/10.3109/03005364000000132>
- 695 Luo, H., Liu, Z., Poeppel, D., 2010. Auditory Cortex Tracks Both Auditory and Visual Stimulus Dynamics Using
696 Low-Frequency Neuronal Phase Modulation. *PLoS Biol.* 8, e1000445.
697 <https://doi.org/10.1371/journal.pbio.1000445>
- 698 Mégevand, P., Mercier, M.R., Groppe, D.M., Golumbic, E.Z., Mesgarani, N., Beauchamp, M.S., Schroeder,
699 C.E., Mehta, A.D., 2020. Crossmodal Phase Reset and Evoked Responses Provide Complementary
700 Mechanisms for the Influence of Visual Speech in Auditory Cortex. *J. Neurosci.* 405597.
701 <https://doi.org/10.1101/405597>
- 702 Metzger, B.A., Magnotti, J.F., Wang, Z., Nesbitt, E., Karas, P.J., Yoshor, D., Beauchamp, M.S., 2020.
703 Responses to Visual Speech in Human Posterior Superior Temporal Gyrus Examined with iEEG

- 704 Deconvolution. *J. Neurosci.* 40, JN-RM-0279-20. <https://doi.org/10.1523/jneurosci.0279-20.2020>
- 705 Meyer, L., Henry, M.J., Gaston, P., Schmuck, N., Friederici, A.D., 2017. Linguistic bias modulates
706 interpretation of speech via neural delta-band oscillations. *Cereb. Cortex* 27, 4293–4302.
707 <https://doi.org/10.1093/cercor/bhw228>
- 708 Nichols, T., Holmes, A., 2003. Nonparametric Permutation Tests for Functional Neuroimaging. *Hum. Brain*
709 *Funct. Second Ed.* 25, 887–910. <https://doi.org/10.1016/B978-012264841-0/50048-2>
- 710 Nidiffer, A.R., Cao, C.Z., O’Sullivan, A.E., Lalor, E.C., 2021. A linguistic representation in the visual system
711 underlies successful lipreading. *bioRxiv*. <https://doi.org/10.1101/2021.02.09.430299>
- 712 O’Sullivan, A.E., Crosse, M.J., Di Liberto, G.M., Lalor, E.C., 2017. Visual cortical entrainment to motion and
713 categorical speech features during silent lipreading. *Front. Hum. Neurosci.* 10, 1–11.
714 <https://doi.org/10.3389/fnhum.2016.00679>
- 715 Obleser, J., Kayser, C., 2019. Neural Entrainment and Attentional Selection in the Listening Brain. *Trends*
716 *Cogn. Sci.* 23, 913–926. <https://doi.org/10.1016/j.tics.2019.08.004>
- 717 Oganian, Y., Chang, E.F., 2019. A speech envelope landmark for syllable encoding in human superior
718 temporal gyrus. *Sci. Adv.* 5, 1–14. <https://doi.org/10.1126/sciadv.aay6279>
- 719 Oldfield, R.C., 1971. The assessment and analysis of handedness: The Edinburgh inventory.
720 *Neuropsychologia* 9, 97–113. [https://doi.org/10.1016/0028-3932\(71\)90067-4](https://doi.org/10.1016/0028-3932(71)90067-4)
- 721 Oostenveld, R., Fries, P., Maris, E., Schoffelen, J.-M., 2011. FieldTrip: Open source software for advanced
722 analysis of MEG, EEG, and invasive electrophysiological data. *Comput. Intell. Neurosci.* 2011, 156869.
723 <https://doi.org/10.1155/2011/156869>
- 724 Ozker, M., Yoshor, D., Beauchamp, M.S., 2018. Frontal cortex selects representations of the talker’s mouth
725 to aid in speech perception. *Elife* 7, 1–14. <https://doi.org/10.7554/eLife.30387>
- 726 Park, H., Ince, R.A.A., Schyns, P.G., Thut, G., Gross, J., 2018. Representational interactions during
727 audiovisual speech entrainment: Redundancy in left posterior superior temporal gyrus and synergy in
728 left motor cortex. *PLOS Biol.* 16, e2006558. <https://doi.org/10.1371/journal.pbio.2006558>
- 729 Park, H., Kayser, C., Thut, G., Gross, J., 2016. Lip movements entrain the observers’ low-frequency brain
730 oscillations to facilitate speech intelligibility. *Elife* 5. <https://doi.org/10.7554/eLife.14521>
- 731 Paulesu, E., Perani, D., Blasi, V., Silani, G., Borghese, N.A., De Giovanni, U., Sensolo, S., Fazio, F., 2003. A
732 functional-anatomical model for lipreading. *J. Neurophysiol.* 90, 2005–2013.
733 <https://doi.org/10.1152/jn.00926.2002>
- 734 Pekkola, J., Ojanen, V., Autti, T., Jääskeläinen, I.P., Möttönen, R., Tarkiainen, A., Sams, M., 2005. Primary
735 auditory cortex activation by visual speech: An fMRI study at 3 T. *Neuroreport* 16, 125–128.
736 <https://doi.org/10.1097/00001756-200502080-00010>
- 737 Plass, J., Brang, D., Suzuki, S., Grabowecky, M., 2020. Vision perceptually restores auditory spectral
738 dynamics in speech. *Proc. Natl. Acad. Sci. U. S. A.* 117, 16920–16927.
739 <https://doi.org/10.1073/pnas.2002887117>
- 740 Rauschecker, J.P., 2012. Ventral and dorsal streams in the evolution of speech and language. *Front. Evol.*

- 741 Neurosci. 4, 5–8. <https://doi.org/10.3389/fnevo.2012.00007>
- 742 Ross, L.A., Saint-Amour, D., Leavitt, V.M., Javitt, D.C., Foxe, J.J., 2007. Do you see what I am saying?
743 Exploring visual enhancement of speech comprehension in noisy environments. *Cereb. Cortex* 17,
744 1147–1153. <https://doi.org/10.1093/cercor/bhl024>
- 745 Sams, M., Aulanko, R., Hämäläinen, M., Hari, R., Lounasmaa, O. V., Lu, S.T., Simola, J., 1991. Seeing speech:
746 visual information from lip movements modifies activity in the human auditory cortex. *Neurosci. Lett.*
747 127, 141–145. [https://doi.org/10.1016/0304-3940\(91\)90914-F](https://doi.org/10.1016/0304-3940(91)90914-F)
- 748 Schroeder, C.E., Lakatos, P., 2009. Low-frequency neuronal oscillations as instruments of sensory selection.
749 *Trends Neurosci.* 32, 9–18. <https://doi.org/10.1016/j.tins.2008.09.012>
- 750 Schroeder, C.E., Lakatos, P., Kajikawa, Y., Partan, S., Puce, A., 2008. Neuronal oscillations and visual
751 amplification of speech. *Trends Cogn. Sci.* 12, 106–113. <https://doi.org/10.1016/j.tics.2008.01.002>
- 752 Scott, S.K., 2019. From speech and talkers to the social world: The neural processing of human spoken
753 language. *Science* (80-). <https://doi.org/10.1126/science.aax0288>
- 754 Stefanics, G., Hangya, B., Hernadi, I., Winkler, I., Lakatos, P., Ulbert, I., 2010. Phase Entrainment of Human
755 Delta Oscillations Can Mediate the Effects of Expectation on Reaction Speed. *J. Neurosci.* 30, 13578–
756 13585. <https://doi.org/10.1523/JNEUROSCI.0703-10.2010>
- 757 Suess, N., Hauswald, A., Reisinger, P., Rösch, S., Keitel, A., Weisz, N., 2022. Cortical Tracking of Formant
758 Modulations Derived from Silently Presented Lip Movements and Its Decline with Age. *Cereb. Cortex*
759 1–16. <https://doi.org/10.1093/cercor/bhab518>
- 760 Sumbly, W.H., Pollack, I., 1954. Visual Contribution to Speech Intelligibility in Noise. *J. Acoust. Soc. Am.* 26,
761 212–215. <https://doi.org/10.1121/1.1907309>
- 762 Teng, X., Tian, X., Doelling, K., Poeppel, D., 2018. Theta band oscillations reflect more than entrainment:
763 behavioral and neural evidence demonstrates an active chunking process. *Eur. J. Neurosci.* 48, 2770–
764 2782. <https://doi.org/10.1111/ejn.13742>
- 765 Teoh, E.S., Cappelloni, M.S., Lalor, E.C., 2019. Prosodic pitch processing is represented in delta-band EEG
766 and is dissociable from the cortical tracking of other acoustic and phonetic features. *Eur. J. Neurosci.*
767 50, 3831–3842. <https://doi.org/10.1111/ejn.14510>
- 768 Tivadar, R.I., Gaglianese, A., Murray, M.M., 2020. Auditory Enhancement of Illusory Contour Perception.
769 *Multisens. Res.* 34, 1–15. <https://doi.org/10.1163/22134808-bja10018>
- 770 Tivadar, R.I., Retsa, C., Turoman, N., Matusz, P.J., Murray, M.M., 2018. Sounds enhance visual completion
771 processes. *Neuroimage* 179, 480–488. <https://doi.org/10.1016/j.neuroimage.2018.06.070>
- 772 Tzourio-Mazoyer, N., Landeau, B., Papathanassiou, D., Crivello, F., Etard, O., Delcroix, N., Mazoyer, B., Joliot,
773 M., 2002. Automated anatomical labeling of activations in SPM using a macroscopic anatomical
774 parcellation of the MNI MRI single-subject brain. *Neuroimage* 15, 273–289.
775 <https://doi.org/10.1006/nimg.2001.0978>
- 776 van Bree, S., Sohoglu, E., Davis, M.H., Zoefel, B., 2020. Sustained neural rhythms reveal endogenous
777 oscillations supporting speech perception, *PLoS Biology*. <https://doi.org/10.1101/2020.06.26.170761>

- 778 Van Veen, B.D., Van Drongelen, W., Yuchtman, M., Suzuki, A., 1997. Localization of brain electrical activity
779 via linearly constrained minimum variance spatial filtering. *IEEE Trans. Biomed. Eng.* 44, 867–880.
780 <https://doi.org/10.1109/10.623056>
- 781 Velleman, P.F., Welsch, R.E., 1981. Efficient computing of regression diagnostics. *Am. Stat.* 35, 234–242.
782 <https://doi.org/10.1080/00031305.1981.10479362>
- 783 Yu, C., Zhou, Y., Liu, Y., Jiang, T., Dong, H., Zhang, Y., Walter, M., 2011. Functional segregation of the human
784 cingulate cortex is confirmed by functional connectivity based neuroanatomical parcellation.
785 *Neuroimage* 54, 2571–2581. <https://doi.org/10.1016/j.neuroimage.2010.11.018>
- 786 Zion Golumbic, E., Cogan, G.B., Schroeder, C.E., Poeppel, D., 2013. Visual input enhances selective speech
787 envelope tracking in auditory cortex at a “Cocktail Party.” *J. Neurosci.* 33, 1417–1426.
788 <https://doi.org/10.1523/JNEUROSCI.3675-12.2013>
- 789 Zuk, N.J., Murphy, J.W., Reilly, R.B., Lalor, E.C., 2021. Envelope reconstruction of speech and music
790 highlights stronger tracking of speech at low frequencies, *PLOS Computational Biology*.
791 <https://doi.org/10.1371/journal.pcbi.1009358>
792